Published in final edited form as:

Biochem Biophys Res Commun. 2017 January 29; 483(1): 258–263. doi:10.1016/j.bbrc.2016.12.156.

Rapid PD-L1 detection in tumors with PET using a highly specific peptide

Samit Chatterjee[1,†], **Wojciech G. Lesniak**[1,†], **Michelle S. Miller**[2], **Ala Lisok**[1], **Emilia Sikorska**[3], **Bryan Wharram**[1], **Dhiraj Kumar**[1], **Matthew Gabrielson**[1], **Martin G. Pomper**[1,4], **Sandra B. Gabelli**[2,5], and **Sridhar Nimmagadda**[1,4,*]

[1]Russell H. Morgan Department of Radiology and Radiological Science, Johns Hopkins University, Baltimore, MD, USA [2]Department of Oncology, Johns Hopkins University, Baltimore MD, USA [3]Faculty of Chemistry, University of Gdańsk, Wita Stwosza 63, 80-308 Gdańsk, Poland [4]Sidney Kimmel Comprehensive Cancer Center, Johns Hopkins University, Baltimore, MD, USA [5]Departments of Medicine and Department of Biophysics and Biophysical Chemistry, Johns Hopkins University, Baltimore, Baltimore, MD, USA

Abstract

Molecular imaging can report on the status of the tumor immune microenvironment and guide immunotherapeutic strategies to enhance the efficacy of immune modulation therapies. Imaging agents that can rapidly report on targets of immunomodulatory therapies are few. The programmed death ligand 1 (PD-L1) is an immune checkpoint protein over-expressed in several cancers and contributes to tumor immune suppression. Tumor PD-L1 expression is indicative of tumor response to PD-1 and PD-L1 targeted therapies. Herein, we report a highly specific peptide-based positron emission tomography (PET) imaging agent for PD-L1. We assessed the binding modes of the peptide WL12 to PD-L1 by docking studies, developed a copper-64 labeled WL12 ([^{64}Cu]WL12), and perform its evaluation *in vitro*, and *in vivo* by PET imaging, biodistribution and blocking studies. Our results show that [^{64}Cu]WL12 can be used to detect tumor PD-L1 expression specifically and soon after injection of the radiotracer, to fit within the standard clinical workflow of imaging within 60 min of administration.

Graphical Abstract

*Correspondence to: Sridhar Nimmagadda, Ph.D., Johns Hopkins Medical Institutions, 1550 Orleans Street, CRB II, #491, Baltimore, MD 21287, Phone: 410-502-6244, Fax: 410-614-3147, snimmag1@jhmi.edu.
†equal contribution

COI: The authors declare no conflicts of interest.

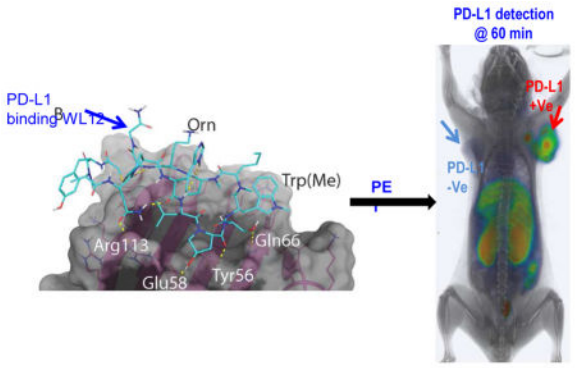

Keywords

immunotherapy; immune checkpoint; diagnostics; peptides; PD-1

INTRODUCTION

Immunotherapy, which harnesses one's own immune system to kill cancer cells, is playing a central role in the treatment of various cancers [1]. In spite of the significantly improved therapeutic outcomes, many cancers do not respond to immunomodulatory therapies. Existing companion diagnostics that work through immunohistochemistry (IHC) provide only a snapshot of the dynamic tumor immune milieu and often do not accurately predict treatment response[2]. Non-invasive imaging technologies can provide quantitative, real-time assessment of tumor biology and guide drug development [3]. Positron emission tomography (PET), the most molecular and quantitative of translational imaging technologies, has been used for repetitive measurement of overall target expression in lesions [3]. PET tracers that can provide rapid and real-time assessment of target expression relevant to immunomodulatory therapies could significantly benefit ongoing clinical trials.

The immune checkpoint protein, programmed death ligand 1 (PD-L1), is a preferred target for immunotherapy. PD-L1 is expressed by a variety of tumors, and its over-expression is induced in tumor cells as an adaptive mechanism in response to tumor infiltrating cytotoxic T-cells[1]. Increased PD-L1 in the tumor microenvironment (TME) causes immune suppression by deactivation of immune infiltrates via binding to programmed cell death protein 1 (PD-1) receptor, expressed by active immune infiltrates [1, 4]. Currently, immunohistochemical (IHC) detection is the best-studied predictive biomarker for therapeutic monitoring of PD-L1/PD-1 targeted therapies [5], but this approach and its available FDA-approved diagnostic *IHC tests for* PD-L1 have significant limitations [6], hampered by inconsistent definitions of antigen-positivity, discordant detection antibodies, insufficient inter-assay agreement, and intra- and inter-tumoral heterogeneities that compromise accuracy and reliability, and thus therapeutic decision-making. Also, tissue samples acquired by biopsy for testing are typically very limited, and may be needed for molecular profiling to identify targetable oncogenic mutations in other pathways (e.g. epidermal growth factor receptor (EGFR), anaplastic lymphoma kinase, DNA repair genes) that confer sensitivity or resistance to existing therapies. Such precious samples make it

often impractical to perform multiple PD-L1 assessments for reliable representation of PD-L1 expression. We anticipate that novel PET imaging agents that enable non-invasive assessment of PD-L1 expression levels, dynamics and distribution, and do so within the standard clinical workflow of imaging within 60 min of administration, will overcome the shortcomings of available (IHC-based) methods for evaluating PD-L1 expression status.

We and others have shown that radiolabeled anti-PD-L1 antibodies can be used to assess PD-L1 expression non-invasively in human tumor xenografts and in syngeneic tumor models [7–13]. Although radiolabeled antibody conjugates are increasingly used for imaging tumor-specific proteins, longer clearance times, extending up to days, are required for enhanced contrast and lesion detection[14]. The dynamic nature of the tumor immune microenvironment provides rationale for development of PET tracers that allow for rapid evaluation of TME. In this regard, low molecular weight, peptide-based PET tracers are desirable candidates for clinical application due to their fast clearance and synthetic tractability[15]. Peptide-based PET tracers targeting somatostatin receptors and chemokine receptor 4 (CXCR4) produce high target-to-non-target ratios in patients[16]. Recently, peptides that specifically bind to PD-L1 have been reported[17], however, their potential to detect PD-L1 expression *in vivo* has not been established. We hypothesized that those PD-L1 binding peptides have the potential to detect PD-L1 expression in tumors rapidly and with high specificity. To test our hypothesis we selected a peptide, WL12 (Fig. 1A), from a reported peptide library that is most suitable for conjugation and possesses a single primary amine and assessed its binding mode to PD-L1. We conjugated a DOTAGA chelator to WL12 for radiolabeling with ^{64}Cu to generate [^{64}Cu]WL12, assessed binding affinities of the peptide derivatives to PD-L1, and determined the *in vitro* uptake of [^{64}Cu]WL12 in cell lines with variable PD-L1 expression. As proof-of-concept we evaluated the ability of the [^{64}Cu]WL12 to detect PD-L1 expression *in vivo* by PET imaging in NSG mice harboring Chinese hamster ovary (CHO) tumors with constitutive human PD-L1 expression (hPD-L1) and isogenic negative control tumors (CHO). Tissue distribution and target specificity of [^{64}Cu]WL12 were confirmed by *ex vivo* biodistribution and blocking studies.

MATERIALS AND METHODS

Supporting information

Detailed procedures for synthesis of WL12-D, WL12-Cu, and their characterization (Fig. S1, S3–S6), method and results of circular dichroism studies (Fig. S2), methods for flow cytometry, competitive inhibition, and *in vitro* binding assay with [^{64}Cu]WL12 can be found in supplementary information.

Materials

PD-L1 binding peptide, WL12, was custom synthesized by CPC Scientific (Sunnyvale, CA) with >95% purity. All other chemicals were purchased from Sigma-Aldrich or Fisher Scientific unless otherwise specified. 2,2′,2″-(10-(2,6-dioxotetrahydro-2H-pyran-3-yl)-1,4,7,10-tetraazacyclododecane-1,4,7-triyl)triacetic acid (DOTAGA anhydrate) and [^{64}Cu]Cl_2 were purchased from CheMatech Macrocycle Design Technologies (catalog # C109; Dijon, France) and The University of Wisconsin, respectively. All cell culture related

reagents were purchased from Invitrogen. Polyclonal anti-human IgG-Eu^{3+}Cryptate (catalog # 61HFCKLA) and XL665-conjugated mouse monoclonal anti-6Histidine antibody (catalog # 61HISXLA) were purchased from Cisbio Assays (Bedford, MA). Recombinant Human PD-1 Fc chimera Protein (catalog # 1086-PD-050) and recombinant human PD-L1(B7-H1)-His-tag protein (catalog #9049-B7) were obtained from R&D systems (Minneapolis, MN).

Docking studies

In order to perform the docking of WL12 to PD-L1, the crystal structure of human PD-1 bound to PD-L1 (PDB ID: 4ZQK) was used as a template. The model was first prepared using the Protein Preparation Wizard in Maestro (Schrödinger Release 2016-2: Maestro, version 10.6, Schrödinger, LLC, New York, NY, 2016) [18]. This involves the assignment of bond orders and formal charges, the addition of hydrogen atoms and the addition of missing side-chains. The hydrogen bonding network within the protein is optimized (including the reorientation of thiol and hydroxyl groups, sampling Asn, Gln and His side chains, and the prediction of the protonation states of His, Asp and Glu), followed by a brief minimization. The structure of PD-1 was removed. A conformational search was performed on the structure of WL12 using Prime Conformational Search (Schrödinger Release 2016-2: Prime, version 4.4, Schrödinger, LLC, New York, NY, 2016). The 100 lowest energy conformers were selected for docking experiments. Docking was performed with Glide (Schrödinger Release 2016-2: Glide, version 7.1, Schrödinger, LLC, New York, NY, 2016) using default settings and input ring conformations [19, 20]. Software used for these computations was curated by SBGrid [21].

PD-L1 and PD-1 binding inhibition assay

A competitive inhibition assay for PD-L1 binding to PD-l was optimized from a previously described fluorescence resonance energy transfer (FRET)-based assay in discussion with Cisbio [22] using PD-1-Ig and PD-L1-His-tag that were detected by anti-human IgG-Eu^{3+} cryptate (IgG-Eu, final concentration 2 nM) and anti-6HIS-XL665 monoclonal antibody using a Perkin Elmer Victor3 1420 multi-label counter (Perkin Elmer, Waltham, MA).

Generation of [^{64}Cu]WL12

$^{64}CuCl_2$ was evaporated to a small volume and transformed into $^{64}Cu(OAc)_2$ by titrating with 0.1 M sodium acetate solution. For radiolabeling, approximately 10 μg of WL12D (4.27 nmol) in 100 μL of sodium acetate was mixed with ~185 MBq (~5 mCi) of $^{64}Cu(OAc)_2$ and incubated at 65 °C for 30 min. Resulting radiotracer was purified on a C-18 (Luna, 5 μm, 10 x 250 mm; Phenomenex) column using a Varian ProStar system equipped with a radioactive single-channel radiation detector and a UV absorbance detector set to 280 nm. Gradient elution starting with 2% methanol (0.1% TFA) reaching 90% methanol over 70 min at flow rate of 5 mL/min with water (0.1% TFA) as co-solvent was applied. [^{64}Cu]WL12 was collected at ~56.2 min (rt for unlabeled peptide: 53.6 min) evaporated, diluted with saline containing 5% DMSO and two drops of Tween 20, used for *in vitro* and *in vivo* evaluation. [^{64}Cu]WL12 was obtained in 52.09 +−6.3% yield with a specific activity of 1.9 ± 0.11 mCi/μg.

Cell lines

Chinese hamster ovary cell line CHO-K1 (henceforth referred to as CHO) and triple negative breast cancer (TNBC) cell line MDAMB231 were purchased from the American Type Culture Collection (ATCC, Manassas, VA) and passaged for fewer than 3 months after which new cultures were initiated from vials of frozen cells. The SUM149 cell line was kindly provided by Dr. Stephen P. Ethier, Medical University of South Carolina, and authenticated by STR profiling at JHU. SUM149 cells were maintained in Ham's F-12 medium with 5% FBS, 1% P/S and 5 μg/mL insulin, and 0.5 μg/mL hydrocortisone. All other cell lines were cultured in ATCC recommended media in an incubator at 37°C in an atmosphere containing 5% CO_2. CHO cell line stably expressing human PD-L1 (henceforth referred to as hPD-L1) was generated in our laboratory[9] and maintained in F-12K medium with 10% FBS, 1% P/S and 2 mg/mL G418.

Animal Models

Animal studies were performed according to the protocols approved by the JHU Animal Care and Use Committee using six-to-eight week old, female, non-obese diabetic severe-combined immunodeficient gamma (NSG) mice obtained from the JHU Immune Compromised Animal Core. Mice were implanted subcutaneously in opposite sides of the upper flanks with 10×10^6 of hPD-L1 and CHO cells. Mice were used for imaging or biodistribution experiments when the tumors reached a volume of 200–300 mm^3.

PET-CT imaging of mouse xenografts

Mice were injected with 150 μCi of [^{64}Cu]WL12 in 200 μL of saline intravenously (n = 3), anesthetized under 3% isofluorane prior to being placed on the scanner. PET images were acquired in two bed positions at 10 min/bed in an ARGUS small-animal PET/CT scanner (Sedecal, Madrid, Spain) as described previously [13].

Ex vivo biodistribution

Mice harboring hPD-L1 and CHO tumors with high and low PD-L1 expression (n=5), respectively were injected intravenously with 40 μCi of [^{64}Cu]WL12 and biodistribution studies were performed as described previously [13]. For the blocking study, mice were co-injected with 2 mg/kg (50 μg) of unmodified peptide with the radiotracer. The percentage of injected dose per gram of tissue (%ID/g) values were calculated based on signal decay correction and normalization to external [^{64}Cu] standards, which were measured in triplicate. Biodistribution data shown is mean ± the standard error of the mean (SEM).

Data analysis

IC_{50} and K_i values were calculated and statistical analysis was performed using a Prism 6 Software (GraphPad Software, La Jolla, CA). *P*-values < 0.05 were considered to be significant using an unpaired two tailed t-test and the comparative reference was cell line or tumor with low PD-L1 expression. Flow cytometry data was analyzed using FlowJo software (Tree Star, Ashland, OR.). by using Prism 6 software (GraphPad).

RESULTS AND DISCUSSION

WL12 binds PD-L1 in a similar mode to that of PD-1

To assess the binding mode of WL12 to PD-L1, we used the co-crystal structure of human PD-L1 bound to PD-1 (PDB ID: 4ZQK)[23] to dock WL12 in the place of PD-1. Given the structural complexity of the macrocycle, WL12, we first performed a conformational search and selected the top 100 conformers for docking studies. These 100 conformers of WL12 were docked into the PD-1 binding site on PD-L1 using Glide[19, 20]. A single conformer was able to dock successfully. In this pose, WL12 forms a beta sheet like structure with two hydrogen bonds made between the backbone of the two macrocycle strands (Fig. 1B). This conformation is supported by circular dichroism experiments (Fig. S2). An overlay of the structure of PD-1 with the bound WL12 reveals the similarities in binding mode between the two. The two beta strands of PD-1 that form the binding interface with PD-L1 overlap with the pseudo-strands of WL12 (Fig. 1C). The D-leucine of WL12 inserts into the same small, hydrophobic pocket as Ile134 of PD-1, and one of the two norleucine residues bind in the same fashion as Ile126 of PD-1. In addition to these hydrophobic interactions, a number of hydrogen bonds are present between WL12 and PD-L1. The carboxamide of the asparagine on WL12 forms a hydrogen bond with Arg113, the hydroxy-proline interacts with Glu58 and Asp61, one of the backbone carbonyls interacts with Tyr56, and the serine hydroxyl interacts with Gln66. The ornithine residue is exposed and does not participate in binding with PD-L1. This suggests that conjugation of a suitable label via amine-coupling methods would not disrupt WL12 binding to PD-L1.

[^{64}Cu]WL12 shows PD-L1-specific cellular uptake in vitro

The ^{13}ornithine (Orn) primary amine was utilized to conjugate DOTAGA, which was then used to prepare a non-radioactive Cu^{2+} analog (WL12-Cu) and to radiolabel with ^{64}Cu. The resulting WL12D and the corresponding WL12-Cu were purified by HPLC, characterized by mass spectrometry (Fig. S1, S3-S6), and subjected to *in vitro* evaluation. To assess the half-maximal inhibitory concentration (IC_{50}) of WL12 and its derivatives to inhibit PD-L1 interaction with PD-1, we optimized a previously described *in vitro* assay that relies on fluorescence resonance energy transfer[22]. We observed IC_{50} values of 22, 23, and 2.9 nM for WL12, WL12D, and WL12-Cu, respectively (Fig. 2A, Fig. S7, S8 and Table S1). These data indicate that WL12 retains high binding affinity to PD-L1 upon modification of ^{13}Orn side chain with DOTAGA and chelation to Cu^{2+}.

To demonstrate PD-L1 specificity and cell uptake, we generated [^{64}Cu]WL12 with high specific radioactivity (1.9 ± 0.1 mCi/μg) and radiochemical purity (> 95%) (Fig. S9 & 10). hPD-L1 cells incubated with [^{64}Cu]WL12 for 1 h showed > 50% uptake of the incubated dose and a 43-fold increase in bound radioactivity compared to the negative control CHO cells (Fig. 2C). We then tested the binding specificity by incubating hPD-L1 cells with [^{64}Cu]WL12 alone or in the presence of a 1 μM blocking dose of WL12. We observed > 95% reduction in bound [^{64}Cu]WL12 in the presence of the excess non-radioactive peptide, indicating that [^{64}Cu]WL12 binding to PD-L1 is specific (Fig. 2C). We further tested the ability of [^{64}Cu]WL12 to detect endogenous PD-L1 expression in two triple negative breast cancer (TNBC) cell lines, MDAMB231 and SUM149, which show high and low PD-L1

expression respectively (Fig. 2B). Two-fold higher uptake of radioactivity in MDAMB231 cells compared to SUM149 cells further confirmed the specificity of [^{64}Cu]WL12 for PD-L1 (Fig. 2C). Flow cytometry analysis for PD-L1 expression demonstrated the mean fluorescence intensity values in the following order: hPD-L1 > MDAMB231 > SUM149 > CHO, which correlated with the uptake of radioactivity (r = 0.9977, Fig. S11 & 12). Collectively those results demonstrate that [^{64}Cu]WL12 binds cancer cells *in vitro* in a PD-L1 expression-dependent manner.

[^{64}Cu]WL12 specifically accumulates in tumors with high PD-L1 expression

To gain insight into the *in vivo* specificity and distribution of [^{64}Cu]WL12, we performed PET-CT imaging studies in mice harboring hPD-L1 and CHO tumors (n = 4). PET imaging studies showed robust uptake of [^{64}Cu]WL12 in hPD-L1 tumors. The increased uptake in hPD-L1 tumors could be observed as early as 10 min and retained through 120 h post-injection (Fig. 3A) with PD-L1 expression confirmed by IHC (Fig. 3B). In addition to tumors, high uptake was also observed in kidneys and liver. To confirm the PET imaging observations, biodistribution studies were performed at 1 and 2 h after the injection of [^{64}Cu]WL12 (n = 3 and n = 5, respectively). Considering the rapid uptake observed in PD-L1-positive tumors, we surmised that biodistribution at 1 and 2 h would be more informative for the development of an ^{18}F-labeled analog. Consistent with the imaging studies, hPD-L1 tumors demonstrated radioactivity uptake in percentage of injected dose/g (%ID/g) values of 14.9 ± 0.8 at 1 h. By contrast, control CHO tumor uptake was 4.0 ± 0.6 %ID/g (Fig. 4). Uptake in the kidneys and liver was also relatively high, with uptake values of 34.4 ± 3.1 and 24.2 ± 2.5 %ID/g, respectively. The tumor-to-muscle and tumor-to-blood ratios for hPD-L1 tumors were 25.6 ± 1.9 and 4.7 ± 1.2, respectively, consistent with the ability of [^{64}Cu]WL12 to provide PD-L1 specific images with high signal-to-noise ratios (Fig. 3).

Biodistribution studies performed at 2 h showed a similar profile with a trend towards decreased radioactivity in kidneys, liver and the tumor (Fig. 4). To demonstrate *in vivo* specificity, we co-injected [^{64}Cu]WL12 with excess WL12 (50 μg, 2 mg/kg) and performed biodistribution studies at 2 h. We observed > 75% reduction in %ID/g values in hPD-L1 tumors ($P < 0.0001$) and no significant difference in control CHO tumors. Kidneys also showed reduced uptake. No significant differences in uptake of radioactivity were observed in other tissues. Increased uptake in the liver, a trend often observed with ^{64}Cu-based imaging agents [24], could be due to lipophilicity of the peptide or the dissociation of Cu^{2+} from the chelator and subsequent transchelation to plasma proteins such as albumin and ceruloplasmin [24], which need to be further investigated. Increased kidney uptake also suggests predominantly renal clearance of the peptide, which was found to be stable in human plasma (Fig. S14). Low uptake observed in spleen, thymus and brown fat, tissues that are known to express PD-L1 and reported to show increased radiolabeled antibody uptake [9, 11, 12], suggests that [^{64}Cu]WL12 has very low or no affinity for mouse PD-L1, which was confirmed by *in vitro* and *in vivo* studies performed using mouse mammary carcinoma 4T1 cells (Fig. S13). Further supporting the [^{64}Cu]WL12 specificity to human PD-L1, no significant differences in uptake were noted in those tissues between control and blocking dose groups, except for kidneys. The imaging and biodistribution studies collectively demonstrate that [^{64}Cu]WL12 binds rapidly and specifically to human PD-L1.

In summary, rapid tumor PD-L1 detection and PD-L1 selectivity were demonstrated *in vitro* and *in vivo* with PET using a highly specific PD-L1 binding peptide [^{64}Cu]WL12. The pharmacokinetics and biodistribution of [^{64}Cu]WL12 indicate that PD-L1 detection is feasible to fit within the standard clinical workflow of imaging patients within 60 min of radiotracer administration. Rapid and non-invasive detection of PD-L1 expression in all malignant lesions in entirety provides unprecedented opportunities to stratify patients for immune modulation therapies and to define the distribution of anti-PD-L1 therapeutic antibody as well as its efficacy.

Supplementary Material

Refer to Web version on PubMed Central for supplementary material.

Acknowledgments

We would like thank Dr. Polina Sysa-Shah for her help with PET imaging acquisition and University of Wisconsin Cyclotron team for ^{64}Cu production. Funding for this study was provided by Allegheny Health Network-Johns Hopkins Cancer Research Fund (SN) and NIH R01CA16631 (SN). SBG was supported by NIH P50 CA062924-20 and Allegheny Health Network-Johns Hopkins Cancer Research Fund. Flow cytometry, histology, and imaging resources were supported by NIH P30 CA006973 and NIH P50 CA103175.

References

1. Topalian SL, Taube JM, Anders RA, Pardoll DM. Mechanism-driven biomarkers to guide immune checkpoint blockade in cancer therapy. Nat Rev Cancer. 2016; 16:275–287. [PubMed: 27079802]
2. Mansfield AS, Dong H. Implications of Programmed Cell Death 1 Ligand 1 Heterogeneity in the Selection of Patients With Non-Small Cell Lung Cancer to Receive Immunotherapy. Clin Pharmacol Ther. 2016; 100:220–222. [PubMed: 26916808]
3. Willmann JK, van Bruggen N, Dinkelborg LM, Gambhir SS. Molecular imaging in drug development. Nat Rev Drug Discov. 2008; 7:591–607. [PubMed: 18591980]
4. Okazaki T, Honjo T. PD-1 and PD-1 ligands: from discovery to clinical application. Int Immunol. 2007; 19:813–824. [PubMed: 17606980]
5. Herbst RS, Soria JC, Kowanetz M, Fine GD, Hamid O, Gordon MS, Sosman JA, McDermott DF, Powderly JD, Gettinger SN, Kohrt HE, Horn L, Lawrence DP, Rost S, Leabman M, Xiao Y, Mokatrin A, Koeppen H, Hegde PS, Mellman I, Chen DS, Hodi FS. Predictive correlates of response to the anti-PD-L1 antibody MPDL3280A in cancer patients. Nature. 2014; 515:563–567. [PubMed: 25428504]
6. Roach C, Zhang N, Corigliano E, Jansson M, Toland G, Ponto G, Dolled-Filhart M, Emancipator K, Stanforth D, Kulangara K. Development of a Companion Diagnostic PD-L1 Immunohistochemistry Assay for Pembrolizumab Therapy in Non-Small-cell Lung Cancer. Appl Immunohistochem Mol Morphol. 2016; 24:392–397. [PubMed: 27333219]
7. Heskamp S, Hobo W, Molkenboer-Kuenen JD, Olive D, Oyen WJ, Dolstra H, Boerman OC. Noninvasive Imaging of Tumor PD-L1 Expression Using Radiolabeled Anti-PD-L1 Antibodies. Cancer Res. 2015; 75:2928–2936. [PubMed: 25977331]
8. Maute RL, Gordon SR, Mayer AT, McCracken MN, Natarajan A, Ring NG, Kimura R, Tsai JM, Manglik A, Kruse AC, Gambhir SS, Weissman IL, Ring AM. Engineering high-affinity PD-1 variants for optimized immunotherapy and immuno-PET imaging. Proc Natl Acad Sci U S A. 2015; 112:E6506–6514. [PubMed: 26604307]
9. Chatterjee S, Lesniak WG, Gabrielson M, Lisok A, Wharram B, Sysa-Shah P, Azad BB, Pomper MG, Nimmagadda S. A humanized antibody for imaging immune checkpoint ligand PD-L1 expression in tumors. Oncotarget. 2016; 7:10215–10227. [PubMed: 26848870]
10. Deng R, Bumbaca D, Pastuskovas CV, Boswell CA, West D, Cowan KJ, Chiu H, McBride J, Johnson C, Xin Y, Koeppen H, Leabman M, Iyer S. Preclinical pharmacokinetics,

pharmacodynamics, tissue distribution, and tumor penetration of anti-PD-L1 monoclonal antibody, an immune checkpoint inhibitor. MAbs. 2016; 8:593–603. [PubMed: 26918260]

11. Hettich M, Braun F, Bartholoma MD, Schirmbeck R, Niedermann G. High-Resolution PET Imaging with Therapeutic Antibody-based PD-1/PD-L1 Checkpoint Tracers Theranostics. 2016; 6:1629–1640.
12. Josefsson A, Nedrow JR, Park S, Banerjee SR, Rittenbach A, Jammes F, Tsui B, Sgouros G. Imaging, Biodistribution, and Dosimetry of Radionuclide-Labeled PD-L1 Antibody in an Immunocompetent Mouse Model of Breast Cancer. Cancer Res. 2016; 76:472–479. [PubMed: 26554829]
13. Lesniak WG, Chatterjee S, Gabrielson M, Lisok A, Wharram B, Pomper MG, Nimmagadda S. PD-L1 Detection in Tumors Using [(64)Cu]Atezolizumab with PET. Bioconjug Chem. 2016; 27:2103–2110. [PubMed: 27458027]
14. Pandit-Taskar N, O'Donoghue JA, Durack JC, Lyashchenko SK, Cheal SM, Beylergil V, Lefkowitz RA, Carrasquillo JA, Martinez DF, Fung AM, Solomon SB, Gonen M, Heller G, Loda M, Nanus DM, Tagawa ST, Feldman JL, Osborne JR, Lewis JS, Reuter VE, Weber WA, Bander NH, Scher HI, Larson SM, Morris MJ. A Phase I/II Study for Analytic Validation of 89Zr-J591 ImmunoPET as a Molecular Imaging Agent for Metastatic Prostate Cancer. Clin Cancer Res. 2015; 21:5277–5285. [PubMed: 26175541]
15. Sun X, Li Y, Liu T, Li Z, Zhang X, Chen X. Peptide-based imaging agents for cancer detection. Adv Drug Deliv Rev. 2016
16. Herrmann K, Schottelius M, Lapa C, Osl T, Poschenrieder A, Hanscheid H, Luckerath K, Schreder M, Bluemel C, Knott M, Keller U, Schirbel A, Samnick S, Lassmann M, Kropf S, Buck AK, Einsele H, Wester HJ, Knop S. First-in-Human Experience of CXCR4-Directed Endoradiotherapy with 177Lu- and 90Y-Labeled Pentixather in Advanced-Stage Multiple Myeloma with Extensive Intra- and Extramedullary Disease. J Nucl Med. 2016; 57:248–251. [PubMed: 26564323]
17. Miller, MM., Mapelli, C., Allen, MP., Bowsher, MS., Gillis, EP., Langley, DR., Mull, E., Poirier, MA., Sanghvi, N., Sun, L-Q., Tenney, DJ., Yeung, K-S., Zhu, J., Gillman, KW., Zhao, Q., Grant-Young, KA., Scola, PM. Macrocyclic inhibitors of the PD1/PDL1 and CD80 (B7-1)/PD-L1 protein/protein interactions. Bristol-Myers Squibb Company; USA: 2016. p. 1093
18. Sastry GM, Adzhigirey M, Day T, Annabhimoju R, Sherman W. Protein and ligand preparation: parameters, protocols, and influence on virtual screening enrichments. J Comput Aided Mol Des. 2013; 27:221–234. [PubMed: 23579614]
19. Friesner RA, Banks JL, Murphy RB, Halgren TA, Klicic JJ, Mainz DT, Repasky MP, Knoll EH, Shelley M, Perry JK, Shaw DE, Francis P, Shenkin PS. Glide: a new approach for rapid, accurate docking and scoring. 1. Method and assessment of docking accuracy. J Med Chem. 2004; 47:1739–1749. [PubMed: 15027865]
20. Halgren TA, Murphy RB, Friesner RA, Beard HS, Frye LL, Pollard WT, Banks JL. Glide: a new approach for rapid, accurate docking and scoring. 2. Enrichment factors in database screening. J Med Chem. 2004; 47:1750–1759. [PubMed: 15027866]
21. Morin A, Eisenbraun B, Key J, Sanschagrin PC, Timony MA, Ottaviano M, Sliz P. Collaboration gets the most out of software. Elife. 2013; 2:e01456. [PubMed: 24040512]
22. Woodard LE, De Silva RA, Behnam Azad B, Lisok A, Pullambhatla M, GLW, Mease RC, Pomper MG, Nimmagadda S. Bridged cyclams as imaging agents for chemokine receptor 4 (CXCR4). Nucl Med Biol. 2014; 41:552–561. [PubMed: 25038987]
23. Zak KM, Kitel R, Przetocka S, Golik P, Guzik K, Musielak B, Domling A, Dubin G, Holak TA. Structure of the Complex of Human Programmed Death 1, PD-1, and Its Ligand PD-L1. Structure. 2015; 23:2341–2348. [PubMed: 26602187]
24. Anderson CJ, Ferdani R. Copper-64 radiopharmaceuticals for PET imaging of cancer: advances in preclinical and clinical research. Cancer Biother Radiopharm. 2009; 24:379–393. [PubMed: 19694573]

Highlights

- A highly specific PD-L1 binding peptide, WL12, was developed as a PET imaging agent.
- [^{64}Cu]WL12 demonstrates specific binding to PD-L1 *in vitro* and *in vivo*
- [^{64}Cu]WL12-PET allows PD-L1 detection in cancers within 60 min of administration
- WL12 binding interactions with PD-L1 overlaps with that of PD-1

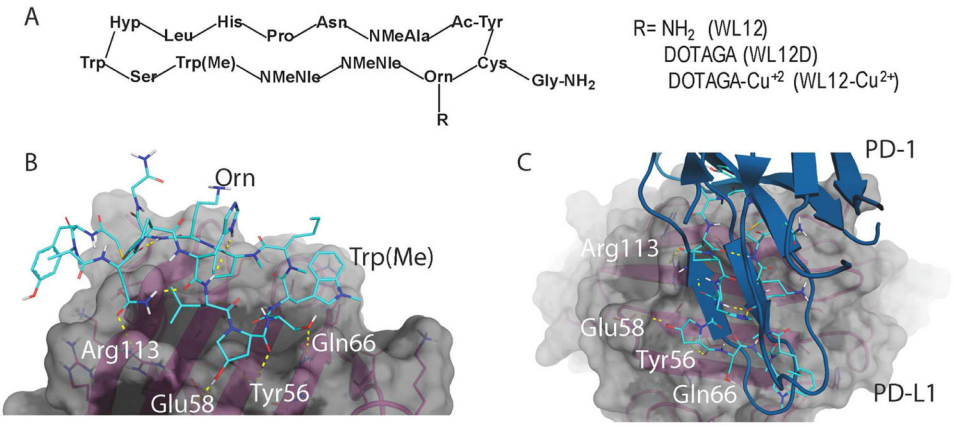

Figure 1. WL12 binding interactions with PD-L1 overlaps with that of PD-1

A, Structural representation of WL12 and its analogs; **B**, Predicted binding mode of WL12 to PD-L1. WL12 forms a beta sheet-like structure in the groove of PD-L1. WL12 is shown in cyan. The surface representation of PD-L1 is shown in gray, with the ribbons and key side chains shown in magenta; **C**, WL12 mimics PD-1 binding to PD-L1. The structure of PD-1 is shown in teal. The two main interacting beta strands of PD-1 overlap well with the conformation adopted by WL12 bound to PD-L1.

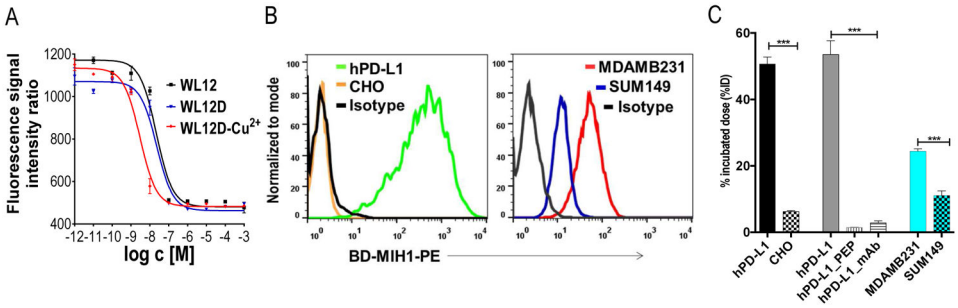

Figure 2. [^{64}Cu]WL12 shows specificity to PD-L1 in vitro

A, Competitive inhibition assay demonstrating the affinity of WL12 analogs for inhibiting PD-1:PD-L1 interaction; **B**, Flow cytometry histograms of cell lines used for *in vitro* studies show variable PD-L1 expression, BD-MIH1-PE is phycoerythryn conjugated anti human PD-L1 antibody; **C**, [^{64}Cu]W12 shows increased binding to cells with high PD-L1 expression which could be blocked by excess peptide (PEP). Significance is indicated by asterisks (*) and the comparative reference is uptake by cell line with low PD-L1 expression or uptake at the blocking dose. *** $P < 0.001$.

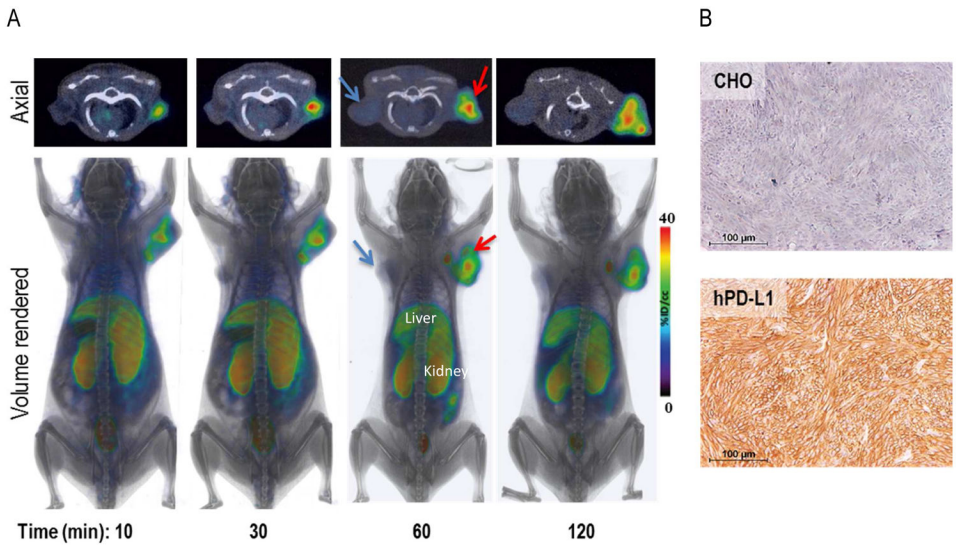

Figure 3. Rapid *in vivo* detection of tumor PD-L1 expression is feasible with [^{64}Cu]WL12

NSG mice with hPD-L1 (red arrow) and CHO tumors (blue arrow) were administered intravenously with 150 μCi of [^{64}Cu]WL12 and images were acquired at 10, 30, 60 and 120 min after the injection of the radiotracer. **A**, Cross sectional (top) and 3D volume rendered (bottom) images show specific accumulation of [^{64}Cu]WL12 in hPD-L1 tumors. **B**, PD-L1 IHC shows strong immunoreactivity (brown color) in hPD-L1 tumors.

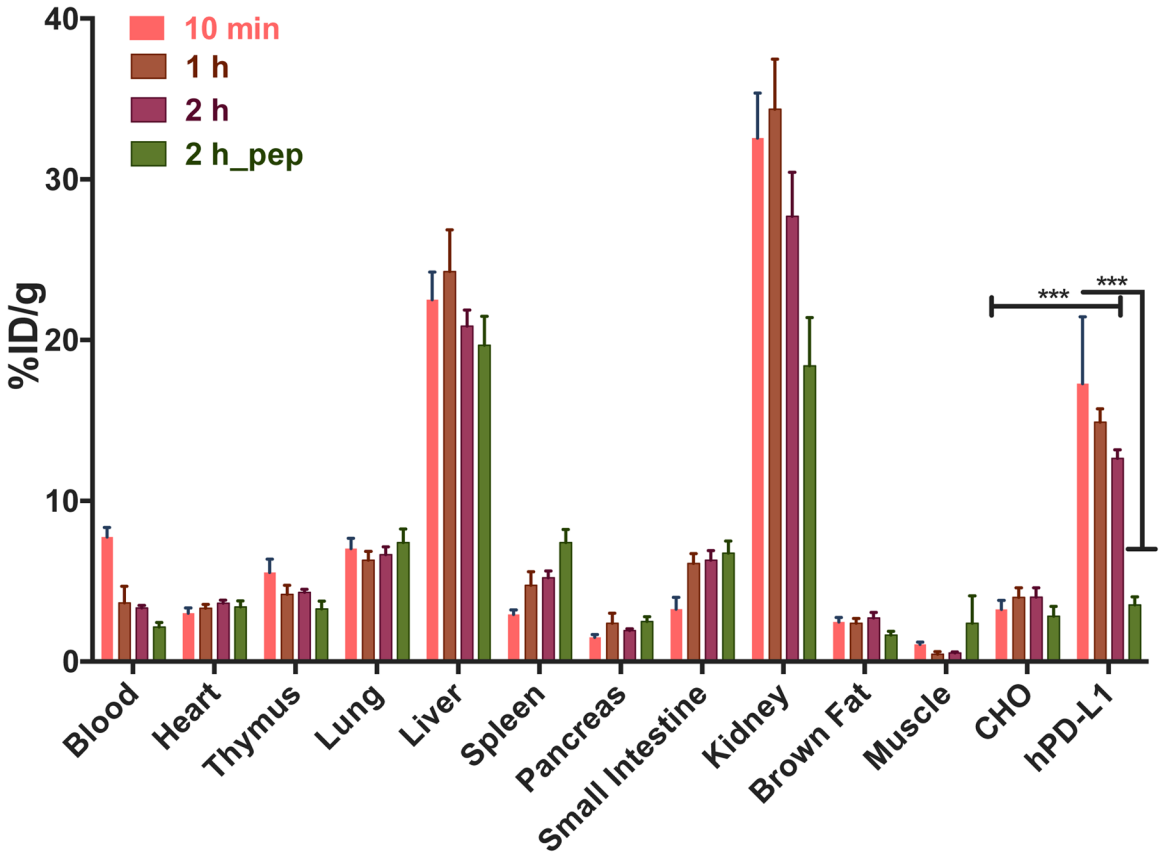

Figure 4. ***Ex vivo*** **biodistribution analysis of [^{64}Cu]WL12 in NSG mice with hPD-L1 and CHO tumors demonstrates specificity**

NSG mice were administered intravenously with 20 μCi of [^{64}Cu]WL12 and tissues were harvested at 60 and 120 min after the injection. For blocking studies mice received excess of peptide (pep) with the radiotracer injection. Significance is indicated by asterisks (*) and the comparative reference is PD-L1 negative tumor uptake at that time point or uptake at the blocking dose. *** $P < 0.001$.